SPG7 Variant Escapes Phosphorylation-Regulated Processing by AFG3L2, Elevates Mitochondrial ROS, and Is Associated with Multiple Clinical Phenotypes

Naif A.M. Almontashiri,[1,2,3] Hsiao-Huei Chen,[4] Ryan J. Mailloux,[2] Takashi Tatsuta,[9] Allen C.T. Teng,[1,2] Ahmad B. Mahmoud,[2] Tiffany Ho,[1] Nicolas A.S. Stewart,[5] Peter Rippstein,[1] Mary Ellen Harper,[2] Robert Roberts,[1] Christina Willenborg,[6] and Jeanette Erdmann[6] for the CARDIoGRAM Consortium, Annalisa Pastore,[7] Heidi M. McBride,[8] Thomas Langer,[9] and Alexandre F.R. Stewart[1,2,*]

[1]Ruddy Canadian Cardiovascular Genetics Centre, University of Ottawa Heart Institute, Ottawa, ON K1Y, Canada
[2]Department of Biochemistry, Microbiology and Immunology, University of Ottawa, Ottawa, ON K1H 8M5, Canada
[3]Center for Genetics and Inherited Diseases, Department of Applied Medical Sciences, Taibah University, Almedinah, P.O. Box 41477, Saudi Arabia
[4]Ottawa Hospital Research Institute, Ottawa, ON K1Y 4E9, Canada
[5]Center for Clinical Pharmacology, Department of Medicine, University of Pittsburgh, Pittsburgh, PA 15261, USA
[6]University of Lübeck, Lübeck 23562, Germany
[7]National Institute for Medical Research, The Ridgeway, Mill Hill, London NW7 1AA, UK
[8]McGill University, Montreal, QC H3A 0G4, Canada
[9]Institute for Genetics, University of Cologne, Cologne 50674, Germany
*Correspondence: astewart@ottawaheart.ca
http://dx.doi.org/10.1016/j.celrep.2014.03.051

SUMMARY

Mitochondrial production of reactive oxygen species (ROS) affects many processes in health and disease. SPG7 assembles with AFG3L2 into the mAAA protease at the inner membrane of mitochondria, degrades damaged proteins, and regulates the synthesis of mitochondrial ribosomes. SPG7 is cleaved and activated by AFG3L2 upon assembly. A variant in SPG7 that replaces arginine 688 with glutamine (Q688) is associated with several phenotypes, including toxicity of chemotherapeutic agents, type 2 diabetes mellitus, and (as reported here) coronary artery disease. We demonstrate that SPG7 processing is regulated by tyrosine phosphorylation of AFG3L2. Carriers of Q688 bypass this regulation and constitutively process and activate SPG7 mAAA protease. Cells expressing Q688 produce higher ATP levels and ROS, promoting cell proliferation. Our results thus reveal an unexpected link between the phosphorylation-dependent regulation of the mitochondria mAAA protease affecting ROS production and several clinical phenotypes.

INTRODUCTION

Chronic diseases, like type 2 diabetes mellitus (T2DM) or coronary artery disease (CAD), are associated with altered mitochondrial function and elevated reactive oxygen species (ROS) production (Lowell and Shulman, 2005; Madamanchi and Runge, 2007). Mitochondria provide energy (ATP) to the cell through oxidative metabolism at the electron transport chain (ETC). During this process, mitochondria also produce ROS as a by-product. ROS oxidize and damage mitochondrial proteins and DNA. For this reason, mitochondria contain enzymes that eliminate ROS, including superoxide dismutase 2 (SOD2) and peroxiredoxin 3 (Prdx3), to actively maintain a reduced state and the mitochondrial electrochemical potential required for ATP production (Hansen et al., 2006).

Mitochondrial matrix proteins that are damaged from oxidation by ROS are degraded by the Lon protease (Bota and Davies, 2002). In addition, the mAAA (matrix ATPase associated with diverse cellular activities) protease also participates in this process because oxidized mitochondrial proteins accumulate in brain extracts from mice carrying a missense mutation in the core AAA domain of AFG3L2 or in mice deficient in AFG3L2 (Maltecca and Casari, 2010). By sensing and destroying damaged matrix proteins, including the components of the ETC, the mAAA protease performs an essential quality control function (Arlt et al., 1996; Hornig-Do et al., 2012). The mAAA protease also regulates the assembly of mitochondrial ribosomes and the synthesis of respiratory chain subunits within mitochondria (Almajan et al., 2012; Nolden et al., 2005). Thus, by controlling the integrity and assembly of the ETC, the mAAA protease may be uniquely positioned to regulate ROS production. Recent evidence indicates that mitochondrial ROS (mROS) production is actively regulated (Sena and Chandel, 2012) and controls diverse mechanisms such as cell proliferation (Formentini et al., 2012) and the bactericidal activity of macrophages (West et al., 2011).

The mAAA protease is assembled as a homohexamer of AFG3L2 or as a heterohexamer between SPG7 and AFG3L2 (Koppen et al., 2007). AFG3L2 is a self-processing protease that is active upon assembly at the mitochondrial inner

CrossMark

membrane. In contrast, cleavage and processing of SPG7 to a mature active protease require coassembly with AFG3L2 (Koppen et al., 2009). Loss-of-function mutations in *AFG3L2* cause spinocerebellar and spastic ataxia (Di Bella et al., 2010; Pierson et al., 2011). Mutations in *SPG7* (also called paraplegin) cause hereditary spastic paraplegia (HSP), a neurodegenerative disorder characterized by progressive weakness and spasticity of the lower limbs due to degeneration of corticospinal axons (Atorino et al., 2003; Casari et al., 1998). Of note, vascular lesions in the frontal cortex have been detected by functional MRI in some forms of HSP linked to the *SPG7* locus (De Michele et al., 1998).

A protein-coding variant that changes an arginine (R688) to glutamine (Q688) in the highly conserved protease domain of SPG7 was recently associated with resistance to the toxic effects of anticancer drugs (Deeken et al., 2010). This same variant has also been reported to nominally associate with the risk for T2DM (Morris et al., 2012). Here, we report an association of this variant with risk for CAD. Our study revealed that unlike the common form of SPG7 whose cleavage is regulated, the Q688 variant is constitutively cleaved and activated. The Q688 variant rescued a dominant-negative form of AFG3L2. Moreover, the Q688 SPG7 variant increased ROS production, promoting cell proliferation and lowering endothelial nitric oxide bioactivity. Our study provides a regulatory mechanism linking mitochondrial matrix quality control to mROS production.

RESULTS

A Variant of SPG7, Q688, Is Associated with CAD Risk
In a search for protein-coding variants that associate with the risk for CAD, we identified one variant (rs12960) in *SPG7* in the Ottawa Heart Genomics Study (OHGS) genome-wide association study (GWAS): 1,542 cases and 1,455 controls (p = 2.34×10^{-3}), odds ratio (OR) (95% confidence interval [CI]) = 1.235 (1.078–1.415). Carrying this allele forward by meta-analysis of 12 GWASs in the CARDIoGRAM consortium comprising 22,233 CAD cases and 64,764 controls, a consistent suggestive association with CAD was found with a combined association of p = 3.74×10^{-5}, OR (95% CI) = 1.076 (1.039–1.114) (Figures 1A and 1B). This variant replaces a positively charged arginine at position 688 with a neutral glutamine residue (Figure 1C) and occurs at an allele frequency of 13%–15% in the European population. It is noteworthy that R688 is invariant among vertebrates and is not polymorphic in the mouse. Although the Q688 allele did not reach genome-wide significant association with CAD in our study, a survey of the literature showed that this allele is associated with other clinically important phenotypes, including resistance to the chemotherapeutic agent docetaxel (Deeken et al., 2010) and T2DM (Morris et al., 2012). Given the pleiotropic effects of this allele, we pursued its functional characterization.

SPG7 Protein Processing and Maturation Are Enhanced in Individuals Who Carry the Q688 Allele
SPG7, like AFG3L2, undergoes two maturation steps. Upon import into the mitochondrial matrix, the N-terminal signal peptide is cleaved by the mitochondrial-processing peptidase (MPP) (Koppen et al., 2009). A second proteolytic cleavage removes an additional N-terminal fragment upon assembly of SPG7 into the SPG7/AFG3L2 heterohexamer (Koppen et al., 2009). Whereas AFG3L2 is autocatalytic, removing its own N-terminal intermediate peptide, SPG7 is dependent on AFG3L2 to be processed to its mature form. Because SPG7 processing is necessary to activate its protease activity, we examined the pattern of SPG7 processing by immunoblot analysis of peripheral blood mononuclear cells (PBMCs) from genotyped CAD patients. Processing of the SPG7 protein to its shorter mature and proteolytically active form was highly correlated (p = 1.23×10^{-7} by trend test) with the gene dosage of the Q688 variant; with nearly 90% of SPG7 being fully processed in PBMCs of patients homozygous for Q688 (Figures 1D and 1E). In addition to being readily accessible from our GWAS-banked blood samples, PBMCs are relevant for CAD studies because they give rise to macrophages, the inflammatory cells that accumulate cholesterol to become the foam cells of atherosclerotic lesions (Ross, 1999). In addition, several studies have validated changes in PBMC gene expression as sensitive indicators of CAD progression or myocardial infarction (Kiliszek et al., 2012; Wingrove et al., 2008). Although the precise location of the N-terminal cleavage sites has been determined for mouse SPG7 (Koppen et al., 2009), it has not been identified in human SPG7 whose N-terminal sequence is divergent from the mouse. Thus, we assigned the names "precursor," "intermediate," and "mature" based on the molecular weights of the bands in the immunoblot.

Migration and proliferation of arterial smooth muscle cells enlarge the atherosclerotic lesion (Ross, 1999). We obtained primary cultures of human aortic smooth muscle cells (HAoSMCs) from different individuals and found the same correlation with increased processing of SPG7 in the two samples heterozygote for the Q688 variant (Figure 1F). These results show that the Q688 variant is associated with increased processing of SPG7 to its proteolytically active form.

Stable HEK293 Cells Expressing the Q688 SPG7 Variant Also Show Increased SPG7 Maturation
To verify that processing of the Q688 variant is intrinsic to this isoform and to further functionally characterize the Q688 variant, human embryonic kidney 293 (HEK293) cells were stably transfected with lentiviral vectors expressing equal levels of the common R688 allele of SPG7 or the CAD risk variant Q688 (Figures 1G and S1). We chose HEK293 cells because they are easily transfected human cells homozygous for the common allele of SPG7. Isolated mitochondria showed that overexpression of the common form of SPG7 did not affect its processing, whereas overexpression of the Q688 variant markedly increased processing to the mature SPG7. Small hairpin RNA (shRNA) knockdown of SPG7 confirmed the identity of the bands as SPG7 (Figure S2). That SPG7 is largely unprocessed in untransfected HEK293 cells was noted (Figure 1G). We cannot exclude the possibility that the intermediate band is a partially processed fragment and that further N-terminal cleavage occurs. Nonetheless, these cells replicate the phenotype (i.e., increased SPG7 processing) observed in PBMCs and HAoSMCs that carry the Q688 allele. This result indicates that increased processing of
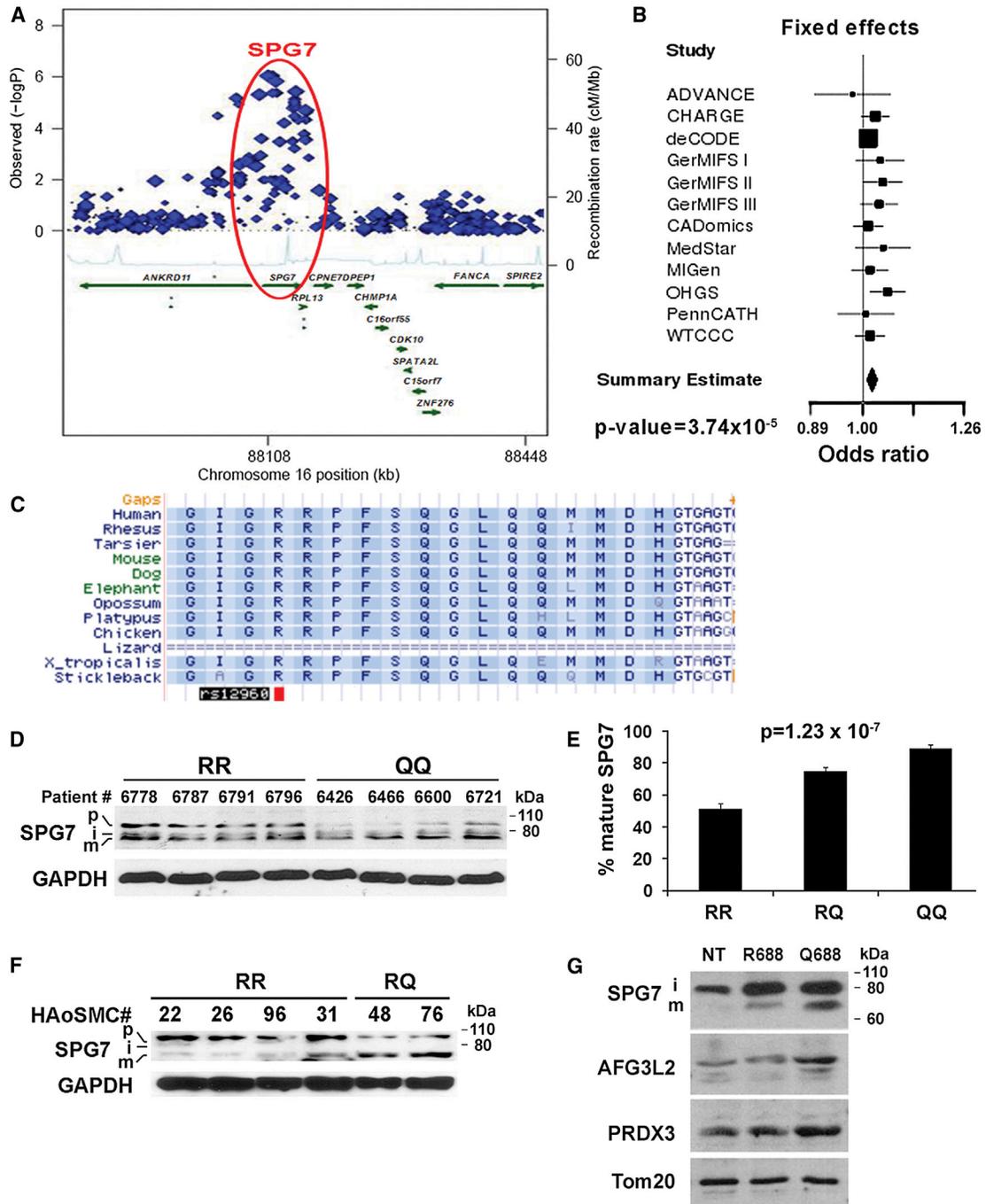
Figure 1. Q688 Variant of *SPG7* Is Associated with Risk for CAD and Alters Proteolytic Processing of SPG7

(A) Cluster of linked SNPs at the SPG7 gene genotyped in CARDIoGRAM (Schunkert et al., 2011).

(B) Meta-analysis of 12 GWASs combining genotype and imputed SNP data from over 22,000 CAD cases and 60,000 controls suggests that the SPG7 locus is associated with CAD ($p = 3.74 \times 10^{-5}$; heterogeneity, $I^2 = 0$).

(C) SNP rs12960 replaces the conserved arginine 688 (R688) with glutamine.

(D) PBMCs from patients with CAD genotyped for rs12960 reveal increased proteolytic processing of SPG7 in Q688 homozygotes (QQ) compared to R688 homozygotes (RR) in whole-cell extracts. Note the increased processing from the precursor (p) and intermediate (i) forms to the mature form (m) in a representative blot.

(E) Quantification of immunoblots, normalized to glyceraldehyde 3-phosphate dehydrogenase (GAPDH) levels, reveals an allele dosage association with the processing of SPG7. RR, (n = 14), RQ, heterozygotes (n = 4), and QQ, homozygotes for the Q688 allele (n = 9).

(F) HAoSMCs genotyped for rs12960 also reveal increased processing to mature SPG7 in heterozygotes (RQ) compared to homozygotes for the common allele (RR) in whole-cell extracts. The identifier for each donor is simplified to the last two digits (see Experimental Procedures for details).

(legend continued on next page)

Q688 SPG7 variant is not due to overexpression or to an extrinsic factor. It is noteworthy that AFG3L2 levels were elevated in cells expressing the Q688 variant but not the common form of SPG7, suggesting that the Q688 variant might stabilize AFG3L2 in the heterohexameric complex. Also of note, Q688 cells had elevated levels of PRDX3, a mitochondrial antioxidant protein that scavenges ROS (Araki et al., 1999).

The Q688 Form of SPG7 Is a Gain-of-Function Variant

Processing of SPG7 to its mature form requires AFG3L2. Therefore, we asked what effect silencing AFG3L2 would have on processing of the common and Q688 variant of SPG7. HEK293 cells expressing the common form of SPG7 accumulated unprocessed protein with AFG3L2 silencing, as expected (Figure 2A). Surprisingly, Q688 was more efficiently processed even when AFG3L2 was knocked down.

Because the SPG7 Q688 variant is more readily processed to its proteolytically active mature form, we used a yeast complementation assay to test whether the Q688 variant could rescue a functionally inactive mutant of AFG3L2. A dominant-negative mutant of AFG3L2 (E691K) that causes spinocerebellar ataxia 28 (SCA28) does not allow mAAA-deficient yeast (lacking both the SPG7 and AFG3L2 homologs) to grow on a nonfermentable carbon source (glycerol) that requires mitochondrial function (Di Bella et al., 2010). This mutant was not rescued by the common form of SPG7 (Di Bella et al., 2010; and also see Figure 2B). Strikingly, growth arrest caused by the AFG3L2 (E691K) mutation was fully rescued by the Q688 SPG7 variant (Figure 2B). Thus, the Q688 variant behaves as a gain of function.

Molecular Modeling Suggests a Stabilizing Influence of the Q688 Variant

We built a 3D model to analyze the impact of the Q688 variant on the structure of the SPG7/AFG3L2 heterohexamer (Figure 3C). Salt bridge formation between residues at the central pore of the heterohexamer could stabilize the complex. The R688 residue in the common form of SPG7 directly faces K415 in AFG3L2, and positive charge repulsion between these two residues is likely attenuated by the spatially proximal E691 of AFG3L2 forming a salt bridge with K415. In contrast, Q688 of the variant makes a salt bridge both with K415 and E691, presumably stabilizing the heterohexamer that could alter the mechanism by which the protease pore functions. To test this hypothesis, we performed native gel electrophoresis (BN-PAGE) and found that cells expressing the Q688 variant had higher levels of SPG7-containing mAAA protease complexes, consistent with increased stabilization by the Q688 variant (Figure 2D).

The Q688 SPG7 Variant Increases ATP Production

Because the SPG7/AFG3L2 mAAA protease requires ATP for its activity (Augustin et al., 2009; Langer, 2000) and participates in

mitochondrial ribosome assembly (Almajan et al., 2012; Nolden et al., 2005) and the degradation of inner membrane proteins (Maltecca and Casari, 2010), we asked whether increased processing and production of the active form of SPG7 by the Q688 variant would increase energy demands and affect ATP production. We performed immunoblot analysis of phosphorylated AMPK (phospho-AMPK) from the mitochondrial extracts of genotyped PBMCs that were used in Figure 1D as well as whole-cell extracts of stably transfected cells. AMPK is a cellular energy sensor that is phosphorylated when ATP levels are inadequate and the ratio of ATP to ADP is low (Hardie, 2003). We observed markedly reduced levels of phospho-AMPK in PBMCs from homozygous carriers of the Q688 variant (Figure 3A). Similarly, cells overexpressing both the common and the variant Q688 forms of SPG7 (Figure 3A) had reduced levels of phospho-AMPK, indicating that these cells have increased ATP production. Although we could not measure ATP production in the frozen banked PBMCs, consistent with the phospho-AMPK results, we found elevated ATP synthesis in mitochondria isolated from stable HEK293 cells overexpressing the common form of SPG7, and even more so the Q688 variant, suggesting increased respiratory activity (Figure 3C). Similarly, mitochondria from primary human umbilical vein endothelial cells (HUVECs) transduced with lentiviral vector expressing the Q688 SPG7 variant also had elevated ATP production (Figure 3D), although HUVECs transduced with the common form (R688) did not have increased ATP production, despite expressing similar levels of SPG7 (data not shown). Uninfected HUVECs were homozygous for the common allele.

The Q688 SPG7 Variant Alters the Stoichiometry of Components of the ETC and Proton Leak from Fatty Acid Oxidation

The mitochondrial ribosome protein Mrpl32 is required for the de novo synthesis of mitochondrially encoded respiratory chain subunits and is a natural target of the mAAA protease (Almajan et al., 2012; Nolden et al., 2005). Upon expression in yeast, loss-of-function mutations in AFG3L2 impair processing of the Mrpl32 precursor leading to respiratory chain deficiencies (Bonn et al., 2010; Di Bella et al., 2010).

Almajan et al. observed decreased levels of mature Mrpl32 in the absence of the m-AAA protease in AFG3L2-deficient cells (Almajan et al., 2012). The increased production of the active form of SPG7 by the Q688 variant was expected to have the opposite effect. Indeed, we found that Mrpl32 processing is enhanced in PBMCs homozygous for the Q688 allele (Figure 3E) as well as in cells expressing the Q688 variant (Figure 3F), indicating increased activity of the m-AAA protease. Surprisingly, although the mitochondrially encoded cytochrome c oxidase 1 (COX1) and COX3, as well as the nuclear-encoded COX4, subunits of complex IV were elevated in cells overexpressing the Q688 variant, COX2 levels were not affected (Figures 3E and 3F). Furthermore, despite COX2 levels not being increased,

---

(G) Mitochondria from stably transformed HEK293 cells expressing the Q688 variant show increased processing to mature SPG7 compared to cells stably expressing the common allele (R688) or nontransfected cells (NT) (n = 4). AFG3L2 levels are increased in cells expressing the variant, as were the levels of PRDX3. TOM20 was used as a mitochondrial loading control protein marker. Overexpression of SPG7 (mature and precursor) was not different for the Q688 and R688 isoforms (Figure S1).
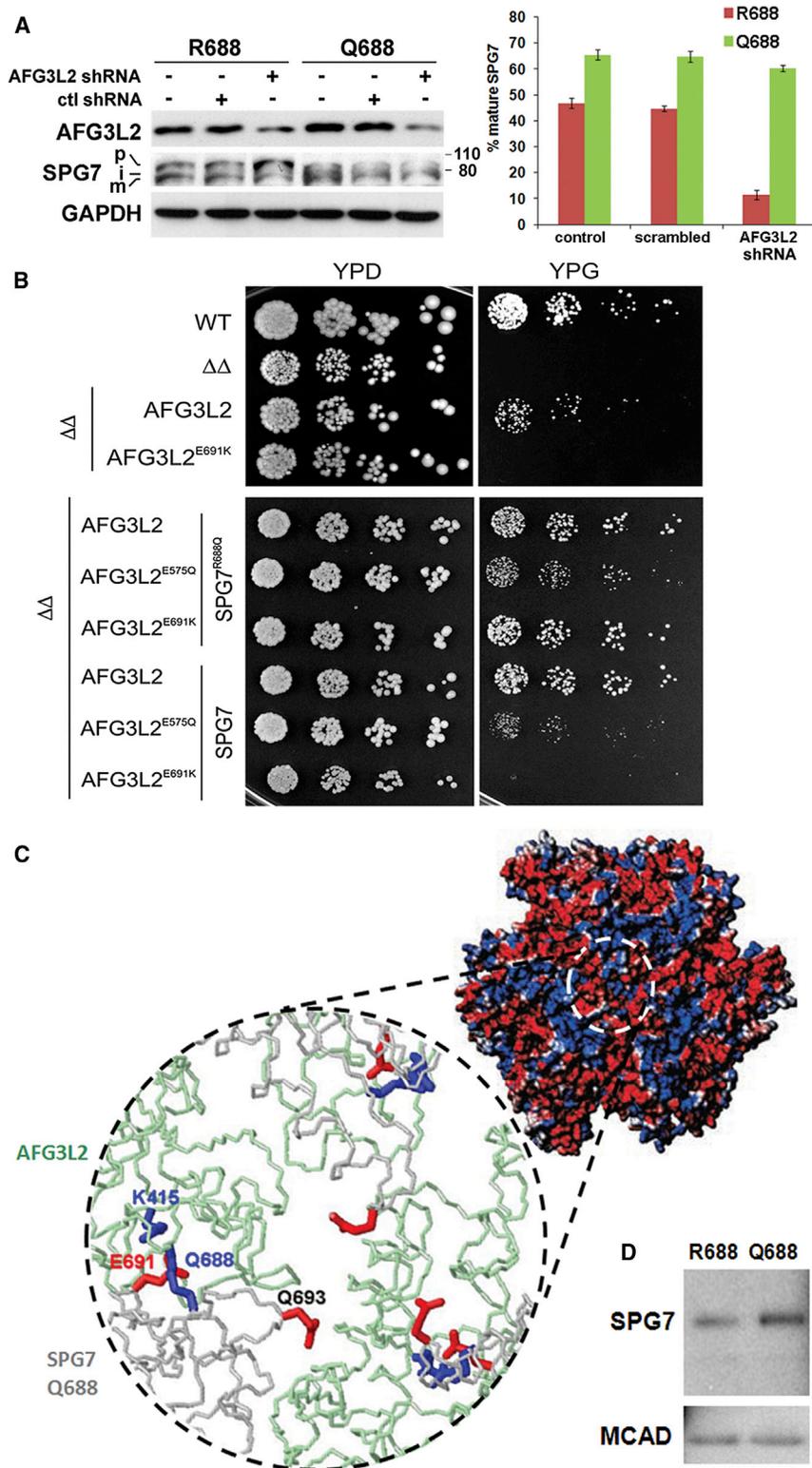
Figure 2. The SPG7 Q688 Variant Rescues Loss-of-Function AFG3L2 Mutants in Yeast

(A) Silencing of AFG3L2 prevents processing of the common form of SPG7, but not the Q688 variant, in whole-cell extracts. Quantification is shown of mature SPG7 as a percentage of total SPG7 (n = 2 experiments).

(B) Complementation studies in *S. cerevisiae* tested for the ability of the Q688 variant (R688Q) to rescue mutant forms of AFG3L2. Serial dilutions of exponentially growing yeast cultures spotted on plates show oxidative growth phenotype of *yta10Δyta12Δ* cells (Δ Δ) expressing normal and mutant human AFG3L2. Respiratory competence is deduced by the ability to grow on 2% glycerol (YPG), a nonfermentable carbon source. The protease-deficient variant of AFG3L2 (E575Q) was partially rescued by the Q688 variant, but the inactivating variant (E691K) was restored to the same extent as cells overexpressing the WT AFG3L2. In contrast, the common form of SPG7 did not rescue the inactivating variant of AFG3L2 (n = 2 experiments, in duplicate).

(C) Model of an SPG7 Q688 and AFG3L2 hetero-hexamer suggests increased stability. Using the structure of the *Thermus thermophilus* AAA protease FtsH as a template (Suno et al., 2006), we modeled the effect of the Q688 variant on a heterohexameric complex with AFG3L2. An enlarged view of the surface representation of the protease face of the AFG3L2/SPG7 heterohexamer (dashed white circle) shows an enlarged wire-frame model of the protease pore. In the common form of SPG7, R688 phases directly K415, a conserved positively charged residue present in AFG3L2, whereas the Q688 residue of the variant SPG7 can form a salt bridge directly with K415.

(D) BN-PAGE immunoblot analysis of supramolecular assembly of SPG7. Blue native electrophoresis of whole-cell extracts from HEK293 cells stably expressing R688 or Q688 showed higher levels of SPG7-containing complexes (~1 MDa) in cells expressing the Q688 variant compared to R688-expressing cells (n = 4). Medium-chain acyl-CoA dehydrogenase (MCAD) was used as BN-PAGE loading control.

dria in cells expressing the Q688 variant (Figure 3H), providing an explanation for elevated ATP production in these cells.

The effect of overexpressing the common and Q688 variant of SPG7 on bioenergetics was further assessed in living cells using a Seahorse analyzer. Cells were fed with glutamine and pyruvate, substrates of the Krebs cycle that generates reduced nicotinamide adenine dinucleotide required for oxidative phosphorylation and ATP production. Cells overexpressing either the common or variant Q688 SPG7 had an increased resting oxygen consumption rate (OCR) in comparison to nontransfected cells (Figure 4A) and increased
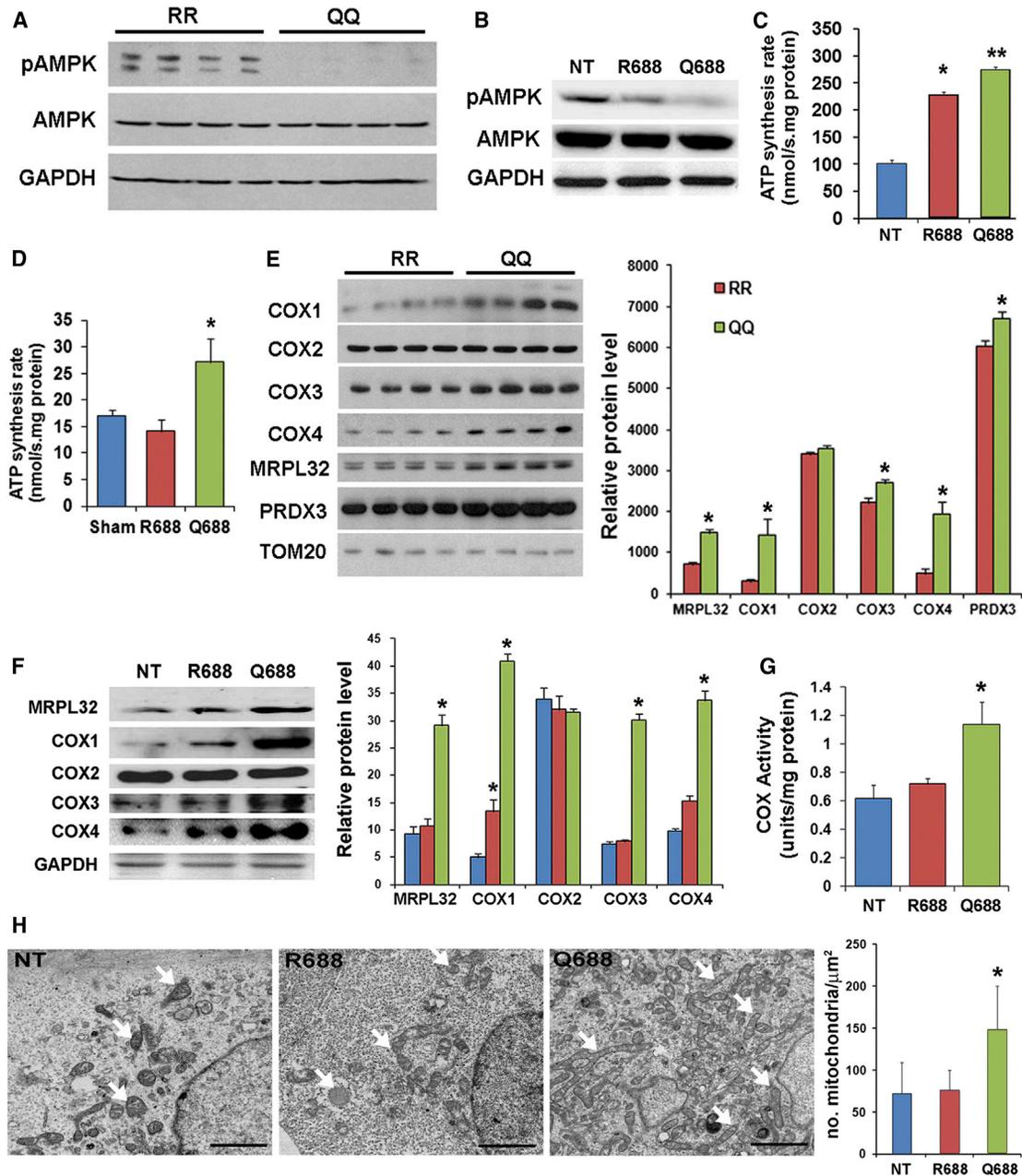
COX activity was elevated in isolated mitochondria expressing the Q688 variant, but not the common form of SPG7 (Figure 3G). Electron microscopy revealed an increased number of mitochon-

Figure 3. The SPG7 Q688 Variant Alters Mitochondrial Bioenergetics

(A and B) Immunoblot analysis showed that phospho-AMPK levels are markedly lower in whole-cell extracts of PBMCs from patients with CAD homozygous for the Q688 variant (A) and in HEK293 cells stably expressing the Q688 variant (B) (n = 3).

(C and D) ATP synthesis was elevated in stably transfected HEK293 cells (C) and in lentiviral-transduced HUVECs (D) expressing Q688. ATP synthesis was measured by a luciferase assay using isolated mitochondria (n = 6). *p < 0.001 compared to control; **p < 0.001 compared to R688.

(E and F) Stoichiometry of complex IV subunits is altered in mitochondrial extracts of PBMCs homozygous for the Q688 variant (E) or in whole-cell extracts of HEK293 cells overexpressing Q688 (F). Levels of Mrpl32 were increased in cells expressing the Q688 variant, indicating increased processing of this ribosomal subunit of mitochondria. However, expression of COX2 was not coordinately upregulated with COX1, COX3, and COX4 in cells expressing the Q688 variant. GAPDH was used as a loading control. Proteins were quantified by densitometry (n = 3). *p < 0.05.

(G) COX activity was elevated in isolated mitochondria of HEK293 cells overexpressing the Q688 variant (n = 3 experiments).

(H) Electron micrographs revealed increased numbers of mitochondria in cells expressing the Q688 variant compared to NT cells or cells expressing the common form of SPG7. Scale bars, 2 μm. Quantification of mitochondrial density (mitochondria/μm² of cytoplasm) was obtained by counting mitochondria (white arrows) from ten individual cells per genotype. Mean ± SEM. *p < 0.001.
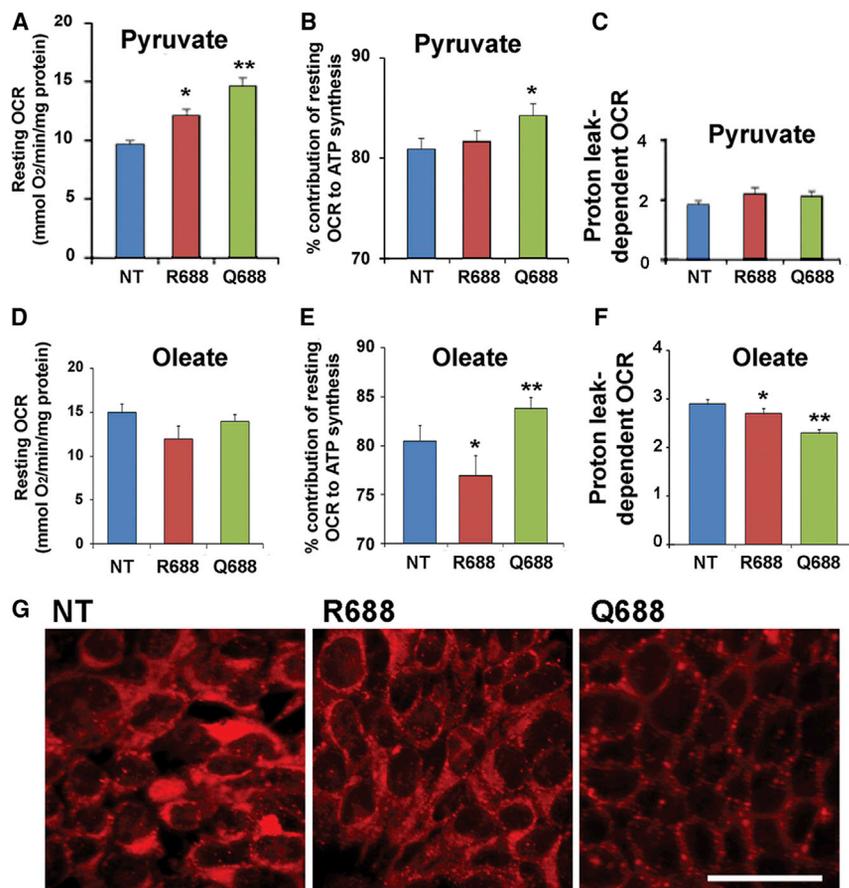
Figure 4. Effect of SPG7 Q688 Variant on Cellular Bioenergetics Measured in Living Cells

Cells were either fed pyruvate (A–C) or oleate (D and E) as substrates.

(A) Resting OCR is elevated in cells expressing the common and variant (Q688) form of SPG7 when fed the TCA cycle substrate pyruvate (n = 4).

(B) Cells expressing the Q688 variant fed pyruvate show an elevated contribution of resting respiration to the aerobic synthesis of ATP (n = 4) (see Figure S1 for details).

(C) Proton leak-dependent OCR was not affected by overexpression of the SPG7 common or variant forms.

(D) A higher-percent contribution of resting OCR to ATP synthesis was observed in cells expressing the Q688 variant when fed oleate (n = 4).

(E) The contribution of resting respiration to aerobic synthesis of ATP was suppressed by overexpression of the R688 form of SPG7 but was elevated by overexpression of the Q688 variant.

(F) Proton leak-dependent OCR in cells expressing the Q688 variant was suppressed (n = 4) (see Figure S1 for details).

In (A)–(F), mean ± SEM.

(G) Cells expressing the Q688 variant accumulate less fatty acid, as indicated by Nile red fluorescence, after 24 hr loading with 100 mM oleate. Scale bar, 50 μm.

$*p < 0.05$; $**p < 0.01$.

carbonilcyanide p-triflouromethoxyphenylhydrazone (FCCP)-stimulated OCR (Figure S3B). Of note, subtracting the proton leak-dependent respiration from resting respiration reveals that cellular respiration associated with ATP synthesis is higher in Q688-expressing cells (Figure S3C). These results agree with the increased ATP synthesis measured in isolated mitochondria. We next determined the contribution of resting respiration toward aerobic ATP synthesis, as an index of energy efficiency, and found that a higher proportion of resting respiration was used to support aerobic ATP synthesis in cells expressing the Q688 variant (Figure 4B). No difference in proton leak-dependent OCR or glycolytic rate was observed between nontransfected and stably transfected cells expressing either the common or Q688 form of SPG7 (Figure 4C). Also, it is important to note that no difference in resting, proton leak-dependent, or FCCP-stimulated respiration was observed in these cells provided with the standard Seahorse glucose-supplemented incubation medium (data not shown). These results indicate that overexpression of the common or the Q688 variant SPG7 does not cause cell stress (Bravo et al., 2011).

Next, we measured the bioenergetics of cells supplied with oleate, a nonfermentable carbon source that requires oxidative metabolism at the mitochondrial matrix (Figures 4D–4F). Intriguingly, no difference in resting respiration was observed between nontransfected cells and cells expressing either the R688 or Q688 variant (Figure 4D). FCCP-stimulated respiration was lower

in cells expressing the R688 and the Q688 form of SPG7 (Figure S4B), whereas no difference in glycolytic rate was observed (Figure S4C). However, cells overexpressing the Q688 variant of SPG7 contributed a larger proportion of oxygen consumption to produce ATP from oleate (Figure 4E). Consistent with this finding, proton leak-dependent respiration was markedly reduced for the Q688-expressing cells (Figure 4F). Because proton leak buffers cellular ROS (Brookes, 2005), this suggests reduced ROS-buffering capacity with oleate. Next, we loaded cells with oleate and observed fewer fat droplets in cells expressing the Q688 variant (Figure 4G). Together, these results show higher fatty acid consumption by β-oxidation and reduced proton leak in cells expressing the Q688 variant, predicting higher ROS production in these cells.

The Q688 SPG7 Variant Increases mROS Levels

Altered ETC protein stoichiometry has been associated with elevated ROS release from mitochondria (Sohal et al., 2008). Furthermore, cells expressing the Q688 variant contributed a larger proportion of mitochondrial respiration to fatty acid oxidation, a known source of ROS (Rosca et al., 2012). We then visualized mROS production using the vital dye MitoSOX Red by fluorescence microscopy and found that HEK293 cells expressing the Q688 variant had markedly elevated ROS production compared to those expressing the common allele (Figure 5A). In addition, we also used the conversion of dihydroethidium to

ethidium that accumulates in the nucleus of stable HEK293 cells actively producing ROS, and confocal time-lapse fluorescent image reconstructions further confirmed that ROS production was mitochondrial by the colocalization of hydroethidium (Het; Figure 5A, red) with MitoTracker (Figure 5A, green) (see Movies S1 and S2). ROS levels were also quantified by a colorimetric assay and found to be elevated in stable HEK293 cells (Figure 5B) and in HUVECs transduced with lentiviral vector (Figure 5C) expressing the Q688 variant. Elevated levels of ROS-scavenging enzyme PRDX3 in PBMCs from patients with CAD homozygous for the Q688 allele (Figure 3E) and in mitochondria from cells expressing the Q688 variant (Figure 1G) were consistent with increased mROS production. Because mitochondrial membrane potential drives mROS production (Echtay et al., 2002), we measured mitochondrial membrane potential using the fluorescent dye tetramethylrhodamine ethyl ester (TMRE) and found that it was elevated in cells expressing the Q688 variant (Figure 5D). ROS production activates endothelial nitric oxide synthase (eNOS) activity, in part by the dephosphorylation of a constitutively phosphorylated inhibitory threonine at position 495 (peNOS-Thr495) (Thomas et al., 2002). PBMCs homozygous for the Q688 variant had markedly reduced peNOS-Thr495 levels (Figure 5E). A similar result was observed in HUVECS transduced with lentiviral vector expressing the Q688 variant (Figure S5). eNOS activation promotes mitochondrial biogenesis (Nisoli et al., 2004), and the levels of the mitochondrial transcription factor A (TFAM) were elevated in PBMCs homozygous for the R688 SPG7 variant (Figure 5E), consistent with increased mitochondrial density observed by electron microscopy in cells overexpressing the R688 variant (Figure 3H). Consistent with the reported effects of mROS and TFAM to stabilize hypoxia-inducible factor 1α (HIF1α) (Bell et al., 2007), we found that cells expressing the Q688 variant had elevated basal HIF1α levels and increased activation of HIF1α in response to hypoxia (Figure 5F).

The Q688 SPG7 Variant Increases Cell Proliferation

Increased mROS production promotes cell proliferation (Formentini et al., 2012), a hallmark of atherosclerotic lesions (Guevara et al., 1999). Given that HEK293 cells expressing the Q688 variant had increased ROS production, we tested whether cell proliferation was also increased. Flow cytometry after bromodeoxyuridine (BrdU) incorporation showed that HEK293 cells expressing the Q688 variant had a 4-fold increase in cell proliferation (Figure 5G). Markers of cellular proliferation, like the proliferating cell nuclear antigen (PCNA), cyclin E, and cyclin D, and the level of phosphorylated retinoblastoma (pRB) were all elevated, whereas the cyclin-dependent kinase inhibitors p27 and p21 were suppressed in these cells (Figure 5H). Addition of the ROS scavengers N-acetyl cysteine (NAC) and Tiron blunted the elevation of PCNA and cyclin E levels (Figure 5I). Thus, these results are consistent with the notion that mROS production controls cellular proliferation (Formentini et al., 2012).

Forskolin Blocks Processing of the R688 SPG7 but Not the Q688 Variant

Next, we asked whether the degree of SPG7 processing might be regulated by the metabolic state, like fasting, when protein kinase A (PKA) is activated (Ritter and Hall, 2009). Activation of PKA by Forskolin in vitro markedly inhibited processing of the common form of SPG7 but had little effect on processing of the Q688 variant (Figure 6A). This indicates that processing of SPG7 is dynamically regulated. To identify a mechanism whereby PKA activation might control SPG7 processing by AFG3L2, we consulted the PhosphoSitePlus databases of curated tandem mass spectrometry sequences (http://www.phosphosite.org/). AFG3L2 contains 3 phosphorylated residues: Y179 (identified in 12 independent reports) in the Fts homology external (FtsH-ext) domain facing the mitochondrial intermembrane space, and T560 (1 report) and S634 (2 reports) on the matrix side (Figure 6B).

PKA activates an unknown tyrosine kinase in the intermembrane space (Lee et al., 2005; Miyazaki et al., 2003). A phospho-peptide of SPG7 phosphorylated at Y195 has been deposited in the PhosphoSitePlus database, but we were unable to confirm this finding by immunoprecipitation or mass spectrometry (data not shown). We therefore examined the possibility that phosphorylation of AFG3L2 regulates SPG7 processing. Immunoprecipitation of AFG3L2 followed by immunoblot analysis using phosphorylated residue-specific antibodies revealed that Forskolin markedly increased phosphorylation of tyrosine residues (Figure 6C). To test whether Y179 of AFG3L2 affects processing of SPG7, we used site-directed mutagenesis to convert this residue to aspartic acid (Y > D, a mutation bearing a negative charge that mimics phosphorylation) or to phenylalanine (Y > F, a residue that cannot be phosphorylated) and tested the effect of overexpression of wild-type (WT) and mutant c-myc-tagged AFG3L2 proteins on endogenous SPG7 processing (Figure 6D). The AFG3L2 Y179D mutation caused accumulation of the intermediate form of SPG7 compared to the WT form of AFG3L2. In contrast, the phosphorylation-dead AFG3L2 mutant Y179F stimulated SPG7 processing. Processing of AFG3L2 was also affected similarly by these mutations, suggesting that phosphorylation of Y179 affects processing of both AFG3L2 and SPG7.

In Figure 7, we propose a model whereby Y179 phosphorylation of AFG3L2 controls processing of the common form of SPG7 (as well as AFG3L2) to regulate mitochondrial bioenergetics and mROS production. The Q688 variant appears to escape the AFG3L2-dependent control mechanism because it is efficiently processed independently of AFG3L2 phosphorylation at Y179 and maintains mitochondria in an energetically activated state.

DISCUSSION

We have characterized Q866 as a gain-of-function variant of SPG7 that causes an increased activity of SPG7-containing mAAA proteases. The SPG7 Q866 variant is efficiently processed independent of phosphorylation of AFG3L2 at Y179, which inhibits processing of SPG7. This increases mROS production, mitochondrial biogenesis, and cellular proliferation. Our data showed that the Q688 variant of SPG7 is a gain of function that rescues a dominant-negative form of AFG3L2 (E691K) associated with SCA28. It will be interesting to determine whether individuals who carry the SCA28 mutation of AFG3L2 (E691K) (Di Bella et al., 2010) and also carry the Q688 variant have an attenuated phenotype relative to individuals homozygous for the common form of SPG7. This could account for the
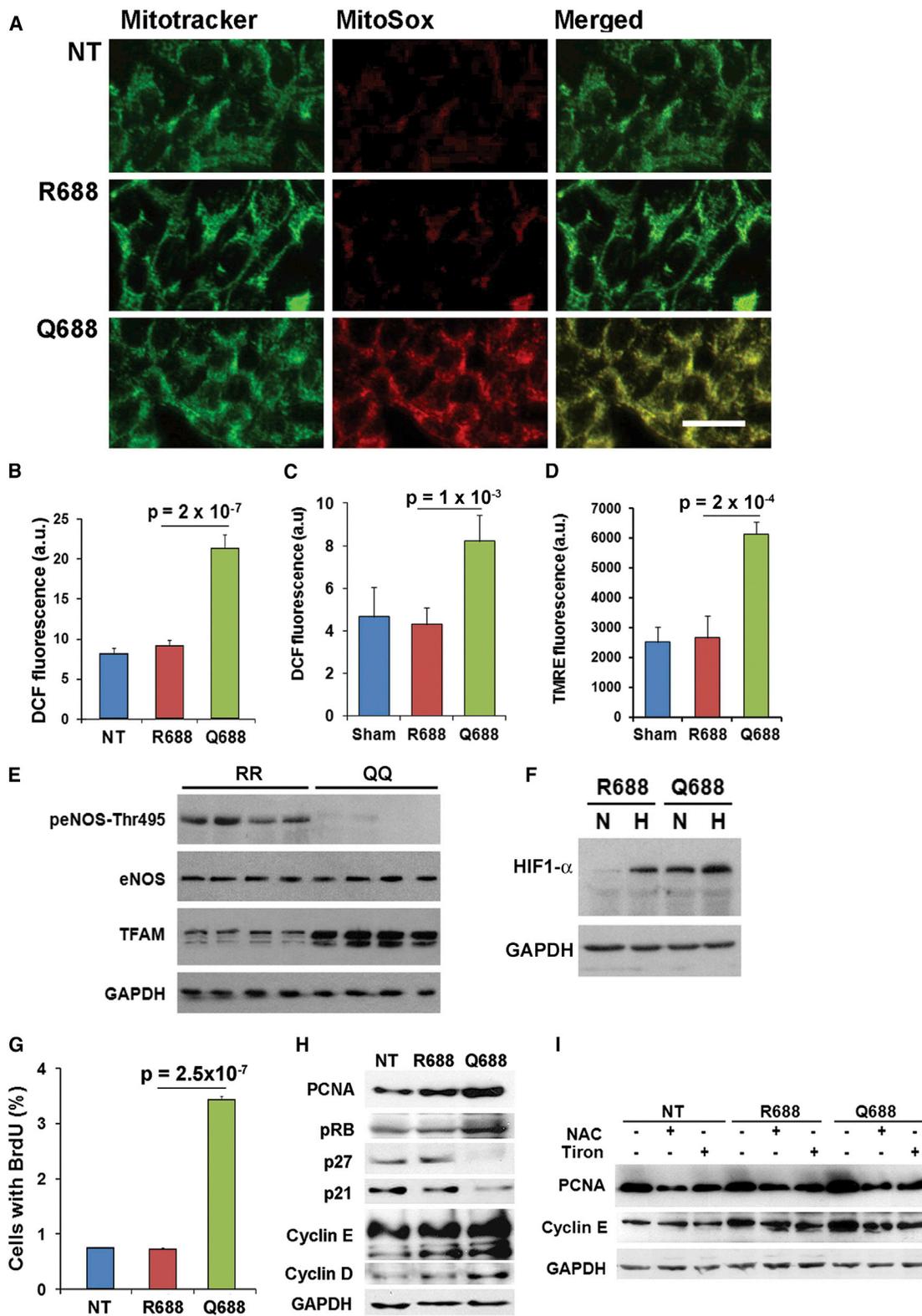
Figure 5. The SPG7 Q688 Variant Increases mROS Production and Cellular Proliferation

(A) mROS was visualized using MitoSOX (red), and mitochondria were visualized using MitoTracker (green). Scale bar, 20 μm.

(B and C) Intracellular ROS measured by DCF fluorescence were highly elevated in HEK293 cells (B) as well as in lentiviral vector-transduced HUVECs (C) expressing the Q688 variant (n = 3 experiments).
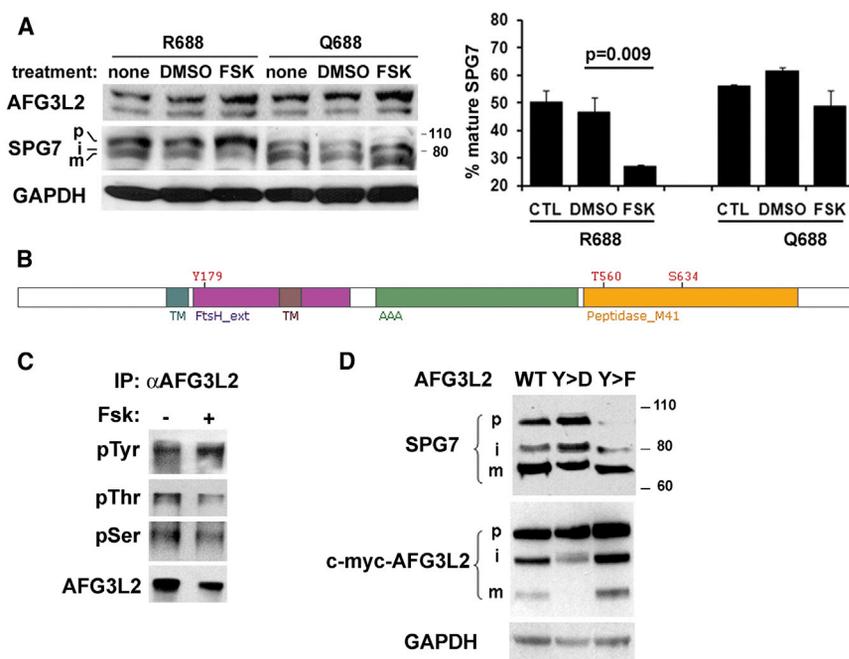
A

Figure 6. SPG7 Processing Is Controlled by AFG3L2 Phosphorylation

(A) Forskolin (FSK) blocks processing of the R688 common form but not the Q688 variant of SPG7. Quantitation of immunoblots (10% acrylamide) showed a significant inhibition of R688 SPG7 processing (n = 3 experiments). Mean ± SEM.

(B) AFG3L2 is phosphorylated at three residues (Y179, T560, and S634), as reported by multiple mass spectrometry studies (http://www.phosphosite.org/).

(C) Forskolin increases tyrosine phosphorylation of AFG3L2. Immunoblots (10% acrylamide) of immunoprecipitated AFG3L2 protein from whole-cell extracts were probed with phosphotyrosine, phosphothreonine, and phosphoserine antibodies. GAPDH antibody confirmed specificity of AFG3L2 immunoprecipitation (Figure S6).

(D) Tyrosine 179 of AFG3L2 regulates SPG7 processing. Site-directed mutagenesis of c-myc-tagged WT AFG3L2 (WT) converted tyrosine 179 to a pseudophosphorylated aspartic acid (Y > D) or to a nonphosphorylatable phenylalanine (Y > F). Immunoblots (6% acrylamide) of whole-cell extracts were probed with antibodies to SPG7, c-myc (to detect overexpressed AFG3L2), and GAPDH to control for loading.

variable penetrance reported for this dominant form of hereditary ataxia (Cagnoli et al., 2006).

The association of the Q688 allele with CAD risk at a level that does not reach genome-wide significance (p = 3.74×10^{-5}) is indicative of the pleiotropic effects of this allele. Indeed, a similar association was reported with the risk for type 2 diabetes in the DIAGRAM consortium (stage 2, OR = 1.05 [1.02–1.08], p = 0.003; n = 75,063) (Morris et al., 2012). Mitochondrial dysfunction and mROS production have been implicated in T2DM (Lowell and Shulman, 2005). A limitation of our study is the lack of data on T2DM in the CARDIoGRAM cohorts. However, because diabetes was an exclusion criterion in the OHGS, the association with CAD and T2DM is likely to be independent.

A recent pharmacogenetic study found that patients with prostate cancer who carry the Q688 variant are more resistant to the toxic effects of anticancer drugs (Deeken et al., 2010). It is likely that the increased ability to detoxify xenobiotic compounds is a direct effect of the Q688 variant. This could explain how this allele has become fixed in the human population. Genes involved in detoxifying xenobiotics evolve more rapidly (Greenberg et al., 2008), presumably because they offer a strong selec-

tive advantage. The Q688 allele shows a similar frequency in Asians as in Europeans (11%–16%) but is rare in black Africans. Although a variant that protects against toxic xenobiotic compounds would confer immediate advantage, the long-term consequence of this gain of protease function may be to increase susceptibility to diseases of aging like CAD and T2DM.

A key finding of our study is that cleavage and activation of SPG7 are regulated processes that can be inhibited by a PKA-like activity. The ability to inhibit the mAAA protease by blocking the cleavage and activation of SPG7 allows cells to regulate mitochondrial protein synthesis and degradation to meet their metabolic needs. Because PKA is a serine/threonine kinase, our data suggest that PKA indirectly inhibits SPG7 processing by activating a tyrosine kinase in the intermembrane space that phosphorylates AFG3L2 at tyrosine 179. Tyrosine kinase activity in mitochondria is located in the intermembrane space (Salvi et al., 2002), and several studies have shown that mitochondrial tyrosine kinase activity modulates cellular metabolism (Hitosugi et al., 2011; Lee et al., 2005; Miyazaki et al., 2003). Although the PhosphoSitePlus repository documents phosphorylation of Y195 in SPG7, we were unable to confirm this finding,

---

(D) Mitochondrial membrane potential measured using the TMRE fluorescent probe showed higher membrane potential in cells expressing the Q688 variant (n = 4 experiments).

In (B)–(D), mean ± SEM.

(E) Immunoblot analysis of whole-cell extracts shows that PBMCs homozygous for the Q688 variant have activated eNOS, as revealed by dephosphorylation of threonine 495 (peNOS-Thr495), and increased levels of TFAM.

(F) Basal and hypoxia-induced (1.5% O_2 for 4 hr) HIF1a levels are higher in cells expressing the Q688 variant (n = 4 experiments).

(G) FACS analysis of BrdU incorporation of synchronized stable HEK293 cells showed increased proliferation of cells expressing the Q688 variant (n = 2 experiments).

(H) Immunoblot analysis revealed elevated levels of cell proliferation markers (PCNA, CyclinE, Cyclin D, and p-RB) and reduced levels of cell-cycle suppressors (p27 and p21) in whole-cell extracts of HEK293 cells stably expressing the Q688 variant (n = 3 experiments). GAPDH verified protein loading.

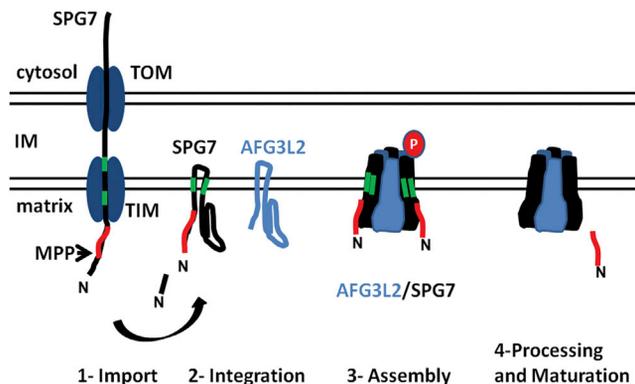(I) ROS scavengers NAC (10 mM) or Tiron (10 mM) restored PCNA and cyclin E levels (n = 3 experiments).

Figure 7. Model of SPG7 Processing

SPG7 preprotein is imported from the cytosol through the intermembrane (IM) space to the mitochondrial matrix, where the signal peptide is cleaved by the MPP. SPG7, like its partner AFG3L2, is somehow anchored through two transmembrane (TM) domains to the inner mitochondrial membrane, with the protease domain facing the matrix. Upon coassembly, tyrosine phosphorylation of AFG3L2 prevents processing of SPG7. Mature SPG7 protein is processed when AFG3L2 is not phosphorylated. The Q688 variant escapes this regulatory process.

suggesting that regulation of SPG7 processing takes place largely through its interaction with AFG3L2. Consistent with this notion, we found that overexpression of a mutant form of AFG3L2 that cannot be phosphorylated at Y179 (Y179F) promoted SPG7 (and AFG3L2) processing. It will be important in future studies to identify the tyrosine kinase and phosphatase that regulate AFG3L2 Y179 phosphorylation and SPG7 processing. The Q688 variant is insensitive to AFG3L2-mediated regulation; this could result from its stabilized interaction with AFG3L2 at the protease pore complex, or if this variant of SPG7 is independent of AFG3L2 (i.e., autocatalytic).

The presence of a constitutively activated mAAA protease in cells expressing the Q688 variant of SPG7 likely leads to an altered stoichiometry of ETC complexes and increased mROS production. Complex IV stoichiometry was similarly altered in PBMCs from patients with CAD homozygous for the Q688 allele as in HEK293 cells overexpressing the Q688 variant, indicating that this is a natural and direct consequence of the Q688 allele. Cellular bioenergetics was affected differently by overexpression of the R688 and Q688 variant of SPG7, in particular in the presence of oleate as a substrate of β-oxidation, a known source of mROS (Rosca et al., 2012). We observed that cells expressing the Q688 variant required a larger proportion of oxygen consumption to produce ATP from oleate and accumulated less oleate in lipid droplets, consistent with increased fatty acid utilization. In addition, these cells displayed reduced proton leak when fed oleate, consistent with reduced ROS-buffering capacity accounting for elevated mROS levels.

Mitochondrial biogenesis was increased in cells expressing the Q688 variant. The mitochondrial count was elevated in electron micrographs, and expression of the TFAM was also elevated in these cells. We observed that expression of Tom20, the mitochondrial translocase of the outer membrane, was not changed

despite increased mitochondrial biogenesis. Of note, during muscle differentiation when mitochondrial biogenesis is activated, Tom20 levels remain relatively unchanged (Grey et al., 2000). Thus, increased mitochondrial biogenesis is not necessarily accompanied by increased Tom20 expression.

Increased mROS production increases cell proliferation (Formentini et al., 2012), and depletion of ROS by NAC induces cell-cycle arrest (Kim et al., 2001). We observed increased proliferation of cells expressing the Q688 variant, and the upregulation of cyclin E and PCNA was reversed by NAC or Tiron, providing direct evidence that mROS drives proliferation in these cells. The altered bioenergetics of mitochondria expressing Q688, in particular the reduced proton efflux when utilizing oleate as a substrate of fatty acid oxidation, is consistent with a reduced ability to buffer ROS, leading to elevated ROS production. Furthermore, elevated mROS production associated with fatty acid oxidation (Yamagishi et al., 2001), increased HIF1α and its associated effect on inflammation (Bartels et al., 2013), and increased cell proliferation are all conditions that would promote coronary atherosclerosis.

The innate immune response is also tied to mROS production. Importantly, the bactericidal activity of macrophages is activated by Toll-like receptors 1, 2, and 4 through elevated mROS production (West et al., 2011). CAD has long been suspected of being linked to bacterial infections and inflammation (Danesh et al., 1997). The Q688 variant, through its effect on elevating mROS production, may promote innate immunity, but at the cost of increased inflammation that contributes to CAD. That PBMCs from patients with CAD homozygous for the Q688 variant showed similar elevations in PRDX3 as seen in cells overexpressing the Q688 variant is consistent with the notion that this allele might augment the inflammatory response.

To date, GWASs have identified more than 40 genetic variants contributing to the risk for CAD (Roberts and Stewart, 2012) but account for only 10% of the CAD heritability. This is due in part to the limited power of the GWAS to discover CAD genetic risk variants that are pleiotropic (Manolio et al., 2009). Pleiotropy occurs when a genetic factor influences more than one physiological trait. Thus, if individuals who have these traits are included in the control group, this would prevent pleiotropic genetic variants that contribute to CAD risk from reaching a level of stringent genome-wide significance ($p < 5 \times 10^{-8}$). Our discovery and functional characterization of the Q688 SPG7 variant as a potential risk factor for CAD and its pleiotropic effects support the notion that much of the missing heritability contributing to the risk for CAD is carried by similar functionally important but pleiotropic alleles.

EXPERIMENTAL PROCEDURES

GWASs

All participants gave written informed consent according to study protocols approved for each of the 12 GWASs as described extensively in the CARDIoGRAM study by Schunkert et al. (2011) and in the Supplemental Experimental Procedures.

Cell Culture, Plasmid Constructs, and Transfection

Details are provided in the Supplemental Experimental Procedures.

Yeast Complementation Assay

Studies in *S. cerevisiae* were carried out as described previously by Bonn et al. (2010) and Koppen et al. (2007) and as detailed in Supplemental Experimental Procedures.

Determination of Mitochondrial H⁺-ATPase Activity

Mitochondria and cytosol were isolated as described by Schauss et al. (2010). Mitochondrial H^+-ATPase activity was measured by fluorescence bioluminescence (A22066; Molecular Probes), as described by Qian et al. (2004) and as detailed in the Supplemental Experimental Procedures.

In Situ Measurement of Cellular Bioenergetics

Mitochondrial bioenergetics and glycolytic flux were tested in intact cells using the Seahorse XF24 Extracellular Flux Analyzer (Seahorse Bioscience, North Billerica), as described previously (Mailloux et al., 2011) and as detailed in the Supplemental Experimental Procedures.

Immunoblot and Immunoprecipitation

Immunoblot and immunoprecipitation protocols and antibodies are described in detail in the Supplemental Experimental Procedures.

Structural Modeling of AFG3L2 and SPG7, Q688, Heterohexamer

Molecular models of AFG3L2 and SPG7 were built as described previously by Di Bella et al. (2010) and in detail in the Supplemental Experimental Procedures.

Intracellular ROS Measurement

The OxiSelect ROS Assay Kit (STA-342; Cell Biolabs) was used to assay ROS activity in HEK293 cells. This is a cell-based assay for measuring activity of ROS using a cell-permeable fluorogenic probe 2′, 7′-dichlorodihydrofluorescein (DCFH) diacetate (DCFH-DA) that is deacetylated by cellular esterases to nonfluorescent DCFH once in the cells. DCFH is rapidly oxidized to highly fluorescent 2′, 7′-dichlorodihydrofluorescein (DCF) by ROS, and fluorescence intensity is proportional to the ROS levels within the cytosol.

Confocal Live Imaging and Videos

Details are provided in the Supplemental Experimental Procedures.

Electron Micrography

Cells were cultured on plastic coverslips, washed in PBS, fixed in 1.6% glutaraldehyde, and were embedded in LR white (Marivac). Thin sections were cut with a Leica Ultracut E ultramicrotome and counterstained with lead citrate and uranyl acetate. Digital images were taken using a JEOL 1230 transmission electron microscope at 60 kV adapted with a 2 × 2 K bottom-mount CCD digital camera (Hamamatsu) and AMT software.

BrdU Staining and Fluorescence-Activated Cell Sorting Analysis

Details are provided in the Supplemental Experimental Procedures.

Mass Spectrometry

Details are provided in the Supplemental Experimental Procedures.

Measurement of Mitochondrial Membrane Potential

The fluorescent probe TMRE (Abcam; ab-113852) was used to measure mitochondrial membrane potential in cells expressing R688 or Q688, as described previously by McClintock et al. (2002).

Cytochrome Oxidase Assay

The determination of COX activity in isolated mitochondria was carried out using the Cytochrome *c* Oxidase Assay Kit according to the manufacturer's protocol (Sigma-Aldrich).

Oleate Loading Assay

HEK293 cells were cultured in modified Eagle's medium containing 10% fetal bovine serum supplemented with 100 mM oleate for 24 hr. Cells were stained with Nile red (Greenspan et al., 1985), and lipid droplets were visualized by fluorescence using a Zeiss AxioImager.Z1 fluorescence microscope.

SUPPLEMENTAL INFORMATION

Supplemental Information includes Supplemental Experimental Procedures, six figures, and two movies and can be found with this article online at http://dx.doi.org/10.1016/j.celrep.2014.03.051.

AUTHOR CONTRIBUTIONS

N.A.M.A., R.J.M., T.T., A.C.T.T., A.B.M., T.H., and N.A.S.S. performed the experiments. M.E.H., J.E., A.P., H.M., and T.L. provided essential data and analysis. N.A.M.A., H.-H.C., R.J.M., A.P., T.L., H.M., R.R., and A.F.R.S. wrote the manuscript.

REFERENCES

Almajan, E.R., Richter, R., Paeger, L., Martinelli, P., Barth, E., Decker, T., Larsson, N.G., Kloppenburg, P., Langer, T., and Rugarli, E.I. (2012). AFG3L2 supports mitochondrial protein synthesis and Purkinje cell survival. J. Clin. Invest. *122*, 4048–4058.

Araki, M., Nanri, H., Ejima, K., Murasato, Y., Fujiwara, T., Nakashima, Y., and Ikeda, M. (1999). Antioxidant function of the mitochondrial protein SP-22 in the cardiovascular system. J. Biol. Chem. *274*, 2271–2278.

Arlt, H., Tauer, R., Feldmann, H., Neupert, W., and Langer, T. (1996). The YTA10-12 complex, an AAA protease with chaperone-like activity in the inner membrane of mitochondria. Cell *85*, 875–885.

Atorino, L., Silvestri, L., Koppen, M., Cassina, L., Ballabio, A., Marconi, R., Langer, T., and Casari, G. (2003). Loss of m-AAA protease in mitochondria causes complex I deficiency and increased sensitivity to oxidative stress in hereditary spastic paraplegia. J. Cell Biol. *163*, 777–787.

Augustin, S., Gerdes, F., Lee, S., Tsai, F.T., Langer, T., and Tatsuta, T. (2009). An intersubunit signaling network coordinates ATP hydrolysis by m-AAA proteases. Mol. Cell *35*, 574–585.

Bartels, K., Grenz, A., and Eltzschig, H.K. (2013). Hypoxia and inflammation are two sides of the same coin. Proc. Natl. Acad. Sci. USA *110*, 18351–18352.

Bell, E.L., Klimova, T.A., Eisenbart, J., Moraes, C.T., Murphy, M.P., Budinger, G.R., and Chandel, N.S. (2007). The Qo site of the mitochondrial complex III is required for the transduction of hypoxic signaling via reactive oxygen species production. J. Cell Biol. *177*, 1029–1036.

Bonn, F., Pantakani, K., Shoukier, M., Langer, T., and Mannan, A.U. (2010). Functional evaluation of paraplegin mutations by a yeast complementation assay. Hum. Mutat. *31*, 617–621.

Bota, D.A., and Davies, K.J. (2002). Lon protease preferentially degrades oxidized mitochondrial aconitase by an ATP-stimulated mechanism. Nat. Cell Biol. 4, 674–680.

Bravo, R., Vicencio, J.M., Parra, V., Troncoso, R., Munoz, J.P., Bui, M., Quiroga, C., Rodriguez, A.E., Verdejo, H.E., Ferreira, J., et al. (2011). Increased ER-mitochondrial coupling promotes mitochondrial respiration and bioenergetics during early phases of ER stress. J. Cell Sci. 124, 2143–2152.

Brookes, P.S. (2005). Mitochondrial H(+) leak and ROS generation: an odd couple. Free Radic. Biol. Med. 38, 12–23.

Cagnoli, C., Mariotti, C., Taroni, F., Seri, M., Brussino, A., Michielotto, C., Grisoli, M., Di Bella, D., Migone, N., Gellera, C., et al. (2006). SCA28, a novel form of autosomal dominant cerebellar ataxia on chromosome 18p11.22-q11.2. Brain 129, 235–242.

Casari, G., De Fusco, M., Ciarmatori, S., Zeviani, M., Mora, M., Fernandez, P., De Michele, G., Filla, A., Cocozza, S., Marconi, R., et al. (1998). Spastic paraplegia and OXPHOS impairment caused by mutations in paraplegin, a nuclear-encoded mitochondrial metalloprotease. Cell 93, 973–983.

Danesh, J., Collins, R., and Peto, R. (1997). Chronic infections and coronary heart disease: is there a link? Lancet 350, 430–436.

Deeken, J.F., Cormier, T., Price, D.K., Sissung, T.M., Steinberg, S.M., Tran, K., Liewehr, D.J., Dahut, W.L., Miao, X., and Figg, W.D. (2010). A pharmacogenetic study of docetaxel and thalidomide in patients with castration-resistant prostate cancer using the DMET genotyping platform. Pharmacogenomics J. 10, 191–199.

De Michele, G., De Fusco, M., Cavalcanti, F., Filla, A., Marconi, R., Volpe, G., Monticelli, A., Ballabio, A., Casari, G., and Cocozza, S. (1998). A new locus for autosomal recessive hereditary spastic paraplegia maps to chromosome 16q24.3. Am. J. Hum. Genet. 63, 135–139.

Di Bella, D., Lazzaro, F., Brusco, A., Plumari, M., Battaglia, G., Pastore, A., Finardi, A., Cagnoli, C., Tempia, F., Frontali, M., et al. (2010). Mutations in the mitochondrial protease gene AFG3L2 cause dominant hereditary ataxia SCA28. Nat. Genet. 42, 313–321.

Echtay, K.S., Murphy, M.P., Smith, R.A., Talbot, D.A., and Brand, M.D. (2002). Superoxide activates mitochondrial uncoupling protein 2 from the matrix side. Studies using targeted antioxidants. J. Biol. Chem. 277, 47129–47135.

Formentini, L., Sánchez-Aragó, M., Sánchez-Cenizo, L., and Cuezva, J.M. (2012). The mitochondrial ATPase inhibitory factor 1 triggers a ROS-mediated retrograde prosurvival and proliferative response. Mol. Cell 45, 731–742.

Greenberg, A.J., Stockwell, S.R., and Clark, A.G. (2008). Evolutionary constraint and adaptation in the metabolic network of Drosophila. Mol. Biol. Evol. 25, 2537–2546.

Greenspan, P., Mayer, E.P., and Fowler, S.D. (1985). Nile red: a selective fluorescent stain for intracellular lipid droplets. J. Cell Biol. 100, 965–973.

Grey, J.Y., Connor, M.K., Gordon, J.W., Yano, M., Mori, M., and Hood, D.A. (2000). Tom20-mediated mitochondrial protein import in muscle cells during differentiation. Am. J. Physiol. Cell Physiol. 279, C1393–C1400.

Guevara, N.V., Kim, H.S., Antonova, E.I., and Chan, L. (1999). The absence of p53 accelerates atherosclerosis by increasing cell proliferation in vivo. Nat. Med. 5, 335–339.

Hansen, J.M., Go, Y.M., and Jones, D.P. (2006). Nuclear and mitochondrial compartmentation of oxidative stress and redox signaling. Annu. Rev. Pharmacol. Toxicol. 46, 215–234.

Hardie, D.G. (2003). Minireview: the AMP-activated protein kinase cascade: the key sensor of cellular energy status. Endocrinology 144, 5179–5183.

Hitosugi, T., Fan, J., Chung, T.W., Lythgoe, K., Wang, X., Xie, J., Ge, Q., Gu, T.L., Polakiewicz, R.D., Roesel, J.L., et al. (2011). Tyrosine phosphorylation of mitochondrial pyruvate dehydrogenase kinase 1 is important for cancer metabolism. Mol. Cell 44, 864–877.

Hornig-Do, H.T., Tatsuta, T., Buckermann, A., Bust, M., Kollberg, G., Rötig, A., Hellmich, M., Nijtmans, L., and Wiesner, R.J. (2012). Nonsense mutations in the COX1 subunit impair the stability of respiratory chain complexes rather than their assembly. EMBO J. 31, 1293–1307.

Kiliszek, M., Burzynska, B., Michalak, M., Gora, M., Winkler, A., Maciejak, A., Leszczynska, A., Gajda, E., Kochanowski, J., and Opolski, G. (2012). Altered gene expression pattern in peripheral blood mononuclear cells in patients with acute myocardial infarction. PLoS One 7, e50054.

Kim, K.Y., Rhim, T., Choi, I., and Kim, S.S. (2001). N-acetylcysteine induces cell cycle arrest in hepatic stellate cells through its reducing activity. J. Biol. Chem. 276, 40591–40598.

Koppen, M., Metodiev, M.D., Casari, G., Rugarli, E.I., and Langer, T. (2007). Variable and tissue-specific subunit composition of mitochondrial m-AAA protease complexes linked to hereditary spastic paraplegia. Mol. Cell. Biol. 27, 758–767.

Koppen, M., Bonn, F., Ehses, S., and Langer, T. (2009). Autocatalytic processing of m-AAA protease subunits in mitochondria. Mol. Biol. Cell 20, 4216–4224.

Langer, T. (2000). AAA proteases: cellular machines for degrading membrane proteins. Trends Biochem. Sci. 25, 247–251.

Lee, I., Salomon, A.R., Ficarro, S., Mathes, I., Lottspeich, F., Grossman, L.I., and Hüttemann, M. (2005). cAMP-dependent tyrosine phosphorylation of subunit I inhibits cytochrome c oxidase activity. J. Biol. Chem. 280, 6094–6100.

Lowell, B.B., and Shulman, G.I. (2005). Mitochondrial dysfunction and type 2 diabetes. Science 307, 384–387.

Madamanchi, N.R., and Runge, M.S. (2007). Mitochondrial dysfunction in atherosclerosis. Circ. Res. 100, 460–473.

Mailloux, R.J., Seifert, E.L., Bouillaud, F., Aguer, C., Collins, S., and Harper, M.E. (2011). Glutathionylation acts as a control switch for uncoupling proteins UCP2 and UCP3. J. Biol. Chem. 286, 21865–21875.

Maltecca, F., and Casari, G. (2010). In vivo detection of oxidized proteins: a practical approach to tissue-derived mitochondria. Methods Mol. Biol. 648, 257–267.

Manolio, T.A., Collins, F.S., Cox, N.J., Goldstein, D.B., Hindorff, L.A., Hunter, D.J., McCarthy, M.I., Ramos, E.M., Cardon, L.R., Chakravarti, A., et al. (2009). Finding the missing heritability of complex diseases. Nature 461, 747–753.

McClintock, D.S., Santore, M.T., Lee, V.Y., Brunelle, J., Budinger, G.R., Zong, W.X., Thompson, C.B., Hay, N., and Chandel, N.S. (2002). Bcl-2 family members and functional electron transport chain regulate oxygen deprivation-induced cell death. Mol. Cell. Biol. 22, 94–104.

Miyazaki, T., Neff, L., Tanaka, S., Horne, W.C., and Baron, R. (2003). Regulation of cytochrome c oxidase activity by c-Src in osteoclasts. J. Cell Biol. 160, 709–718.

Morris, A.P., Voight, B.F., Teslovich, T.M., Ferreira, T., Segrè, A.V., Steinthorsdottir, V., Strawbridge, R.J., Khan, H., Grallert, H., Mahajan, A., et al.; Wellcome Trust Case Control Consortium; Meta-Analyses of Glucose and Insulin-related traits Consortium (MAGIC) Investigators; Genetic Investigation of ANthropometric Traits (GIANT) Consortium; Asian Genetic Epidemiology Network–Type 2 Diabetes (AGEN-T2D) Consortium; South Asian Type 2 Diabetes (SAT2D) Consortium; DIAbetes Genetics Replication And Meta-analysis (DIAGRAM) Consortium (2012). Large-scale association analysis provides insights into the genetic architecture and pathophysiology of type 2 diabetes. Nat. Genet. 44, 981–990.

Nisoli, E., Falcone, S., Tonello, C., Cozzi, V., Palomba, L., Fiorani, M., Pisconti, A., Brunelli, S., Cardile, A., Francolini, M., et al. (2004). Mitochondrial biogenesis by NO yields functionally active mitochondria in mammals. Proc. Natl. Acad. Sci. USA 101, 16507–16512.

Nolden, M., Ehses, S., Koppen, M., Bernacchia, A., Rugarli, E.I., and Langer, T. (2005). The m-AAA protease defective in hereditary spastic paraplegia controls ribosome assembly in mitochondria. Cell 123, 277–289.

Pierson, T.M., Adams, D., Bonn, F., Martinelli, P., Cherukuri, P.F., Teer, J.K., Hansen, N.F., Cruz, P., Mullikin, J.C., for The Nisc Comparative Sequencing Program, and Blakesley, R.W., et al. (2011). Whole-exome sequencing identifies homozygous AFG3L2 mutations in a spastic ataxia-neuropathy syndrome linked to mitochondrial m-AAA proteases. PLoS Genet. 7, e1002325.

Qian, L., Song, X., Ren, H., Gong, J., and Cheng, S. (2004). Mitochondrial mechanism of heat stress-induced injury in rat cardiomyocyte. Cell Stress Chaperones 9, 281–293.

Ritter, S.L., and Hall, R.A. (2009). Fine-tuning of GPCR activity by receptor-interacting proteins. Nat. Rev. Mol. Cell Biol. 10, 819–830.

Roberts, R., and Stewart, A.F.R. (2012). 9p21 and the genetic revolution for coronary artery disease. Clin. Chem. 58, 104–112.

Rosca, M.G., Vazquez, E.J., Chen, Q., Kerner, J., Kern, T.S., and Hoppel, C.L. (2012). Oxidation of fatty acids is the source of increased mitochondrial reactive oxygen species production in kidney cortical tubules in early diabetes. Diabetes 61, 2074–2083.

Ross, R. (1999). Atherosclerosis—an inflammatory disease. N. Engl. J. Med. 340, 115–126.

Salvi, M., Brunati, A.M., Bordin, L., La Rocca, N., Clari, G., and Toninello, A. (2002). Characterization and location of Src-dependent tyrosine phosphorylation in rat brain mitochondria. Biochim. Biophys. Acta 1589, 181–195.

Schauss, A.C., Huang, H., Choi, S.Y., Xu, L., Soubeyrand, S., Bilodeau, P., Zunino, R., Rippstein, P., Frohman, M.A., and McBride, H.M. (2010). A novel cell-free mitochondrial fusion assay amenable for high-throughput screenings of fusion modulators. BMC Biol. 8, 100.

Schunkert, H., König, I.R., Kathiresan, S., Reilly, M.P., Assimes, T.L., Holm, H., Preuss, M., Stewart, A.F.R., Barbalic, M., Gieger, C., et al.; Cardiogenics; CARDIoGRAM Consortium (2011). Large-scale association analysis identifies 13 new susceptibility loci for coronary artery disease. Nat. Genet. 43, 333–338.

Sena, L.A., and Chandel, N.S. (2012). Physiological roles of mitochondrial reactive oxygen species. Mol. Cell 48, 158–167.

Sohal, R.S., Toroser, D., Brégère, C., Mockett, R.J., and Orr, W.C. (2008). Age-related decrease in expression of mitochondrial DNA encoded subunits of cytochrome c oxidase in Drosophila melanogaster. Mech. Ageing Dev. 129, 558–561.

Suno, R., Niwa, H., Tsuchiya, D., Zhang, X., Yoshida, M., and Morikawa, K. (2006). Structure of the whole cytosolic region of ATP-dependent protease FtsH. Mol. Cell 22, 575–585.

Thomas, S.R., Chen, K., and Keaney, J.F., Jr. (2002). Hydrogen peroxide activates endothelial nitric-oxide synthase through coordinated phosphorylation and dephosphorylation via a phosphoinositide 3-kinase-dependent signaling pathway. J. Biol. Chem. 277, 6017–6024.

West, A.P., Brodsky, I.E., Rahner, C., Woo, D.K., Erdjument-Bromage, H., Tempst, P., Walsh, M.C., Choi, Y., Shadel, G.S., and Ghosh, S. (2011). TLR signalling augments macrophage bactericidal activity through mitochondrial ROS. Nature 472, 476–480.

Wingrove, J.A., Daniels, S.E., Sehnert, A.J., Tingley, W., Elashoff, M.R., Rosenberg, S., Buellesfeld, L., Grube, E., Newby, L.K., Ginsburg, G.S., and Kraus, W.E. (2008). Correlation of peripheral-blood gene expression with the extent of coronary artery stenosis. Circ Cardiovasc Genet 1, 31–38.

Yamagishi, S.I., Edelstein, D., Du, X.L., Kaneda, Y., Guzmán, M., and Brownlee, M. (2001). Leptin induces mitochondrial superoxide production and monocyte chemoattractant protein-1 expression in aortic endothelial cells by increasing fatty acid oxidation via protein kinase A. J. Biol. Chem. 276, 25096–25100.